Chemical Physics Letters 511 (2011) 356–362

Contents lists available at ScienceDirect

Chemical Physics Letters

journal homepage: www.elsevier.com/locate/cplett

Study of the growth of conductive single-wall carbon nanotube films with ultra-high transparency

Dachuan Shi, Daniel E. Resasco *

School of Chemical, Biological, and Materials Engineering and Carbon Nanotube Technology Center (CANTEC), University of Oklahoma, 100 E. Boyd, Norman, OK 73019, USA

ARTICLE INFO

Article history:
Received 7 February 2011
In final form 20 June 2011
Available online 28 June 2011

ABSTRACT

We report a study of the growth of conductive single-wall carbon nanotube (SWCNT) films with ultra-high transparency (typically above 98% at 550 nm wavelength) on quartz substrates. Ferritin was used as the catalyst precursor and ethanol as the carbon feed. The effects of experimental parameters on film structure and performance have been investigated. Catalyst concentration and pre-annealing of the substrate after catalyst deposition seem to be important parameters to optimize the resulting films. Analysis of these trends gives further insight into the mechanism of SWCNT film growth and termination, which may contribute to more effective synthesis of SWCNT films.

1. Introduction

One of the most promising applications of single-wall carbon nanotubes (SWCNT) is the fabrication of thin conductive films. Their excellent electrical conductivity and high optical transparency make them attractive coating materials for a large number of devices and may become a potential replacement for indium tin oxide (ITO) glass. Although it is widely used today in most transparent conducting electrodes (TCE), ITO exhibits some limitations for current and future opto-electronic applications. Not only the long-term availability of indium may present a problem, but also technically ITO might be surpassed by SWCNT in aspects such as optical, chemical, and structural performance [1]. Consequently, fabrication methods of TCEs have received extensive attention in recent literature. In the majority of the methods investigated, carbon nanotubes are prepared ex situ and transferred to a substrate as a suspension [2–8]. In general, the as-synthesized SWCNTs are post-treated in order to purify the nanotubes and facilitate the application of the suspension onto the substrate by different techniques, including transfer printing [2,3], filtration [4,5], spray [6], dip-coating [7], and drop casting [8]. Typically, the post-treatment that produces the suspension includes sonication, acid or caustic attack, use of a surfactant, etc. Most of these methods have a negative impact on film performance. Acid or caustic attack and sonication may cut the nanotubes and introduce defects. External surfactants or dispersant may also be detrimental to conductivity. They may be difficult to remove completely and their presence incorporates an electrical barrier that increases the contact resistance between nanotubes, increasing the resistance of the network.

In addition, the as-synthesized SWCNTs are often in the form of bundles and typical post-treatment methods are not effective in de-bundling them. As discussed below, bundling further limits film conductivity and, as a result, it is difficult to produce thin SWCNT films with low sheet resistance [9]. Moreover, in some applications of TCEs, such as display panels, ultra-high transparency is a feature even more desirable than conductivity. But these methods cannot produce films of such high transparency. Therefore, in this contribution, we have explored methods to simultaneously reduce sheet resistance and maximize transparency into the ultra-high region (i.e. >98%).

The approach that we have explored is the in situ production of transparent films. Growth of clean SWCNT arrays grown on flat substrates by chemical vapor deposition (CVD) has been recently reported [10–13]. Relatively long and parallel SWCNTs are grown along specific crystallographic axes of the crystals due to a preferential nanotube-substrate interaction. However, the use of these arrays in TCEs is limited by the anisotropic electrical properties caused by their particular morphology [14,15]. Isotropic thin films appear as a more suitable structure to maximize conductivity at high transparency.

Selection of the catalyst that facilitates the nanotube growth is critical. Depending on reaction conditions, Fe can be effective in catalyzing the selective growth of SWCNT [16]. A common protein, ferritin has been widely used as catalyst precursor, particularly for studies on flat substrates. Ferritin can be conveniently applied onto substrates by dipping [17] or spin-coating [18]. Previous efforts on SWCNTs synthesis involving ferritin include either growing SWCNT arrays on substrates such as ST-cut quartz and sapphire [13,19,20], which result in electrical anisotropy as discussed earlier, or discrete SWCNTs [17,18], which were not continuous enough to form conducting networks. Recently, two-dimensional networks have been grown using ferritin as the catalyst precursor

* Corresponding author. Fax: +1 405 325 5813.
E-mail address: resasco@ou.edu (D.E. Resasco).

0009-2614/$ - see front matter © 2011 Elsevier B.V. All rights reserved.
doi:10.1016/j.cplett.2011.06.057

[21]. However, they were formed on non-transparent silicon substrates, so no optical transmittance test was conducted on them. In addition, the reported sheet resistance was rather high, 770 kΩ/square. In this work, we have found that that ferritin is an effective catalyst precursor when combined with water-doped ethanol as carbon feed. Under these conditions, conductive SWCNT films with ultra-high transparency on transparent quartz substrates have been successfully synthesized. In an effort to optimize the film performance, we tested catalyst annealed in air for different times, as well as using aqueous solutions of ferritin of varying concentrations. Scanning electron microscope (SEM) and Raman spectroscopy were used to characterize the SWCNT films. The optoelectronic performance of the films was monitored by measuring the sheet resistance and optical transmittance on the same samples. The observed relationships between catalyst/SWCNT film structure and growth parameters (annealing time, catalyst concentration) provide further insight toward the tailoring of films with controlled properties.

2. Experimental

Transparent quartz substrates were washed thoroughly with soap and dipped in piranha solution (i.e. one part of hydrogen peroxide in three parts of sulfuric acid) for 15 min at room temperature. After this treatment the samples were rinsed with acetone and isopropanol and blown-dried under nitrogen flow. Ferritin (Type I, saline solution, Sigma–Aldrich) was diluted in distilled water by 10, 30, or 200 times to achieve iron concentrations of 100 mM, 33 mM, and 5 mM (indicated below as C100, C33, and C5). Each solution with the selected ferritin concentration was spin-coated onto the quartz substrate on a spinner (Laurell WS-400-6NPP-LITE) at 5000 rpm for 10 s. The substrate was then dried in a vacuum oven at 90 °C for two hours and annealed in air at 900 °C for a specified time of 0, 10, 20, 30, 45, or 60 min (indicated below as A0, A10, A20, A30, A45, and A60).

Growth of SWCNT films on the quartz/catalyst substrate was carried out in a horizontal furnace (Lindberg/Blue). In each run, the substrate was placed at the center of a one-inch tube reactor and heated up to 925 °C in H_2. Then, ethanol mixed with 0.5% of water was injected at a rate of 0.30 ml/h along with Ar and H_2 (35 sccm total flow, ~3:1 M ratio) for 20 to 30 min. We identify the samples used in this study with the notation Cx – Ay – Rz, where x is the ferritin concentration in mM, y is the annealing time in minutes, and z is the reaction time in minutes.

Sheet resistances were measured on a test meter (JANDEL HM20). Current–voltage measurements were conducted on a Keithley SourceMeter (2410), by applying the electrical probes onto silver electrodes (Ted Pella) painted on the two extremes of the SWCNT film. Transmittance spectra were obtained on a Shimadzu UV–Vis spectrophotometer (UV-2450). Raman spectra were acquired on a Jovin Yvon-Horiba Lab Ram equipped with a charge-coupled detector and a He–Ne laser (632 nm) as excitation source. SEM analysis was carried out on a FEI Quanta 600 field-emission gun environmental scanning electron microscope.

3. Results and discussion

Figure 1 shows a photograph of one of the transparent SWCNT films obtained from a Fe catalyst film prepared from a solution of ferritin (in this case, C33-A60-R30). The SWCNT film exhibited a sheet resistance of 7.1 kΩ/sq and transmittance of 98.4% at 550 nm wavelength, a remarkably high transparency compared to other films [22,23]. The corresponding dc electrical conductivity was calculated to be around 3.9×10^4 S/m, which is twice as that reported for a pure CNT bucky paper [24]. As seen in the image, the substrate with the SWCNT film (right) displays a transparency hardly distinguishable from that of the plain substrate (left), which had a transmittance of 99.5%. The SEM images for this same sample at different magnifications are shown in Figure 2. The low-magnification SEM image (Figure 2A) demonstrates the uniform coverage of the substrate by the SWCNT film. The higher-magnification images (Figure 2B and C) reveal that the film is composed of essentially unbundled and long nanotubes that interconnect and form a continuous network. It is worth noting that, at the acceleration voltage (20 kV) used for all the SEM observations, no charging effect was observed, which is an indication of a high electrical conductivity of the film.

The observed uniformity of the films can be largely attributed to a uniform distribution of the Fe clusters that catalyzed the growth of nanotubes. The uniform distribution of the metal can be attributed to two important aspects of the preparation of the film. The first one is the pretreatment of the surface with piranha solution that renders the substrate highly hydrophilic and the second one is the high spinning speed (5000 rpm) used in the spin-coating step. The long nanotube length and individuality (i.e. no bundling) observed on these SWCNT films are in sharp contrast to those typically observed in films made from solution, in which the nanotubes have been shortened to get dispersed, but tend to form bundles as they dry from the suspension [8]. Theoretical and experimental studies have shown that long and individual SWCNTs have a significant advantage in generating films of high conductivity [2,25–27]. It has been demonstrated that the film resistance is largely dominated by the resistance of the nanotube–nanotube contacts [28]. Therefore, the lower the number of junctions in the film, the higher is the overall conductivity.

The Raman spectrum for the same sample (Figure S1) shows that the intensity ratio between the G band (ca 1582 cm^{-1}, signature of a sp^2 carbon structure) and the D band (ca 1350 cm^{-1}, due to disordered carbon) is high (~16) and indicative of low defect concentration in the nanotube and an overall good quality. And, most importantly, such a high G/D ratio is indicative of SWCNTs rather than MWCNTs (multi-wall carbon nanotubes). The radial breathing mode (RBM) could not be seen due to the strong scattering appearing in this region from the quartz substrate [19].

We have investigated the effect of varying the experimental parameters on the resulting film morphology and, consequently, performance. While there are multiple parameters that could be adjusted, in this study we have focused on systematically varying those that we predict could be most crucial, while keeping the other parameters unchanged. The first parameter that we analyzed is substrate annealing time. In this comparison, we used a C33 ferritin solution and 20 min reaction time while varying the annealing time. The results are summarized in Figure 3. It can be observed that the sheet resistance generally decreases with increased annealing time, from above measurement range of the test meter (~1 Ω/sq – ~10 MΩ/sq) with no annealing to 12.6 kΩ/sq at 60 min. At the same time, the transmittance at 550 nm is seen to gradually and slowly decrease with annealing time from 99.6% at 10 min to 99.3% at 60 min. Interestingly, without annealing, the observed optical transmittance was even lower than with annealing.

To interpret the observed trends, the surface of the films was characterized by SEM (see Figure 4), which helped us evaluate the morphology changes caused by the annealing process. Without annealing of the substrate, no SWCNTs could be observed on the substrate. With 10 min annealing, a rather open network composed of short tubes was obtained, with an approximate surface density of ~5 tubes/μm^2. Starting from 20 min, a denser and more interconnected network was formed as the annealing time increased; the tube surface density was observed to increase by about ten times to ~50 tubes/μm^2, which corresponds well with

Figure 1. Optical photo showing quartz substrates without (left) and with a SWCNT film (right). The black dot on the bottom left corner of the right substrate was used as a marker for the side with the film.

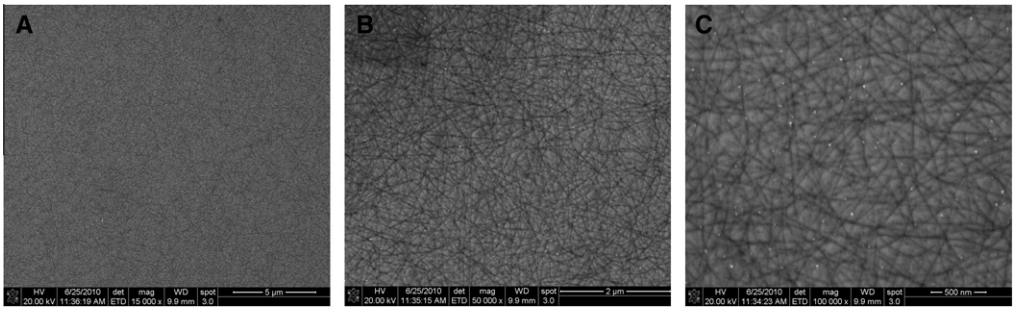

Figure 2. SEM images of the SWCNT film at magnifications of 15 000× (A), 50 000× (B) and 100 000× (C).

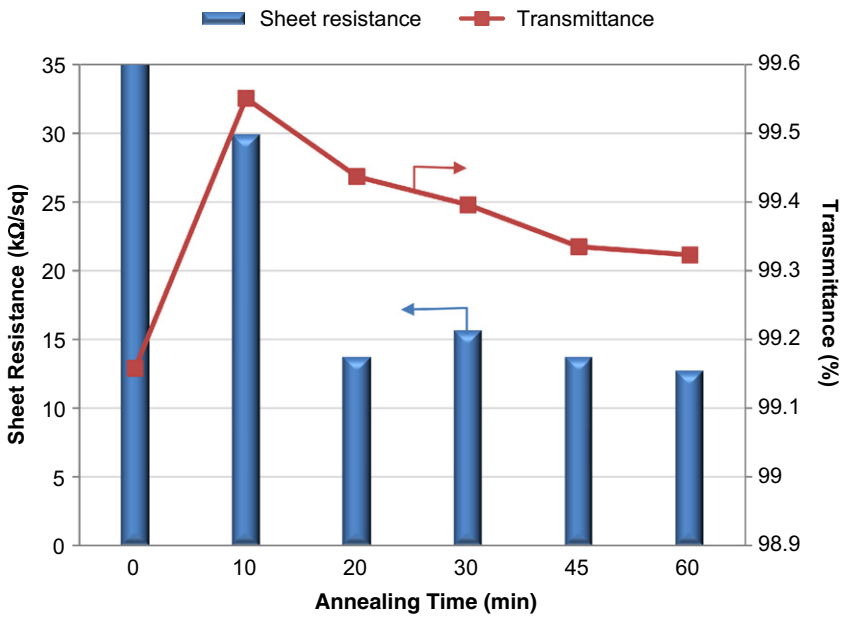

Figure 3. Sheet resistance and transmittance (at 550 nm) as a function of annealing time.

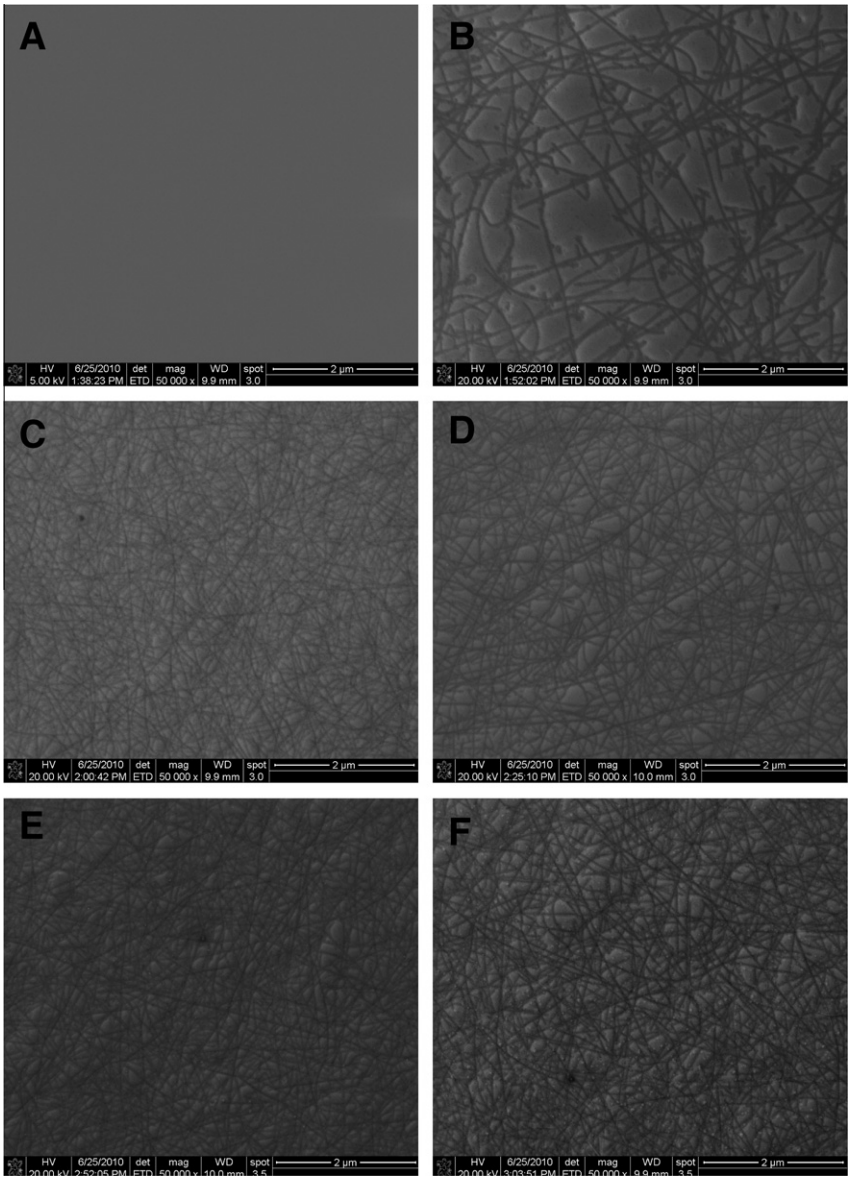

Figure 4. SEM images of SWCNT films obtained with annealing time of 0 min (A), 10 min (B), 20 min (C), 30 min (D), 45 min (E), and 60 min (F).

the increase in film conductivity. The changes in morphology also correspond with the changes in transmittance. That is, the open film obtained with only 10 min annealing time resulted in the lowest SWCNT coverage and highest optical transmittance. Without annealing, an amorphous shell associated with the organic fractions of the ferritin still remained on the substrate, causing deactivation of Fe [29]. In addition, these fragments increase the absorption of light but do not enhance conductivity. Therefore, this sample exhibited high resistance and low optical transmittance.

The clear correlation observed between the catalyst annealing time and the film morphology (performance) can be explained in terms of the process of SWCNT growth and termination. In a recent study on the growth of aligned SWCNTs on ST-cut quartz substrates [30], we have observed that the termination of the nanotube growth was accelerated by nanotube–nanotube interaction that leads to hindrance of the growth and subsequent catalyst deactivation [31]. The introduction of controlled amounts of water was seen to effectively keep the catalyst particles active by gasifying the carbon deposits. We found that including 0.5% water in the liquid feed was efficient to avoid rapid deactivation. While lower water contents caused no noticeable improvement, more water led to complete etching of carbon nanotubes. On the other hand, it is well known that high temperature treatments (e.g. during annealing) lead to metal particle sintering [32]. As can be seen from the higher-magnification SEM images of the annealing series (Figure 5), when the samples were annealed for less than 30 min, the sintering of the catalyst particles did not result in particle growth large enough to be detectable. By contrast, annealing treatments for more extended periods (e.g. 45 and 60 min) led to particles large enough to be clearly observed by SEM.

It is important to point out that annealing time was the only variable changed in this series. That is, the observed decrease in sheet resistance with increasing annealing time must be related to the increasing size of the catalyst particles. It has been previously demonstrated [33–35] that there is a direct correlation between the size of the metal clusters that catalyze the growth of SWCNTs and the nanotube diameters, i.e. larger metal clusters generate nanotubes of larger diameters. Therefore, one needs to explain why this diameter increase causes a corresponding increase in electrical conductivity of the film. Our proposed explanation is

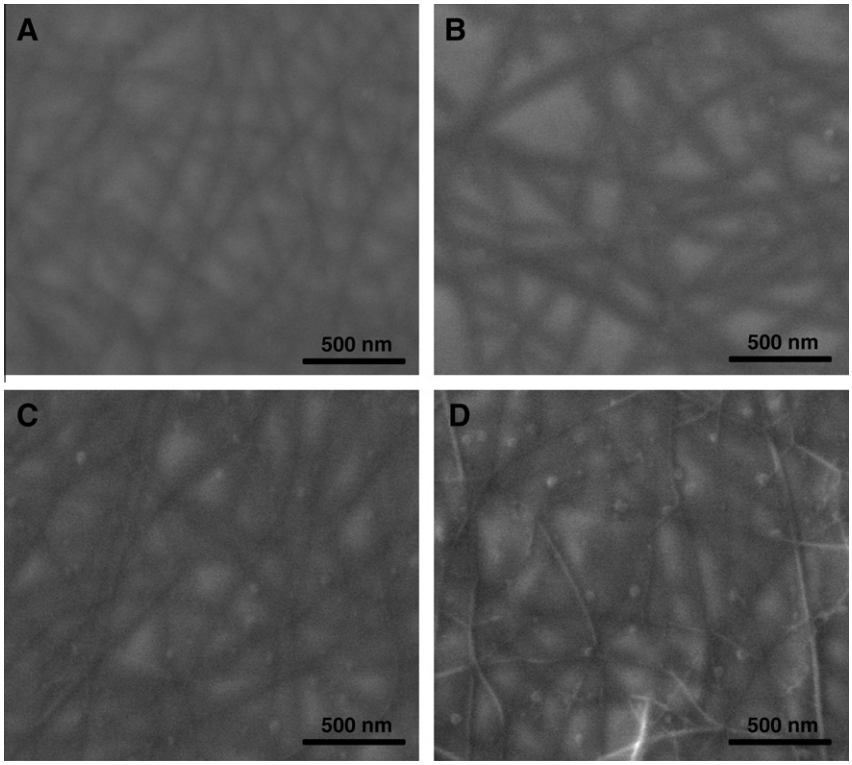

Figure 5. Higher-magnification SEM images of SWCNT films obtained with annealing time of 20 min (A), 30 min (B), 45 min (C), and 60 min (D). Catalyst particles are larger in (C) and (D) in comparison to those in (A) and (B).

that the growth hindrance caused by nanotube–nanotube interaction is less pronounced when the diameter is larger, since larger diameter implies higher nanotube rigidity. Therefore, one can anticipate that these nanotubes should be longer and thus of higher conductivity. At the same time, Dai et al. [36] have shown that contact resistance seems to increase significantly for the small diameter nanotubes.

In addition to investigating the effect of annealing time, we evaluated the effect of varying the metal concentration of the ferritin solution. For this comparison we fabricated films with varying ferritin concentration (C5, C33, and C100), while keeping the rest of the parameters constant. That is, all the samples in this series were subject to 60 min annealing and 30 min reaction. The results of the optoelectronic performance are summarized in Figure 6.

First, it is observed that the optical transmittance of the film decreased with increasing ferritin concentration. The sheet resistance, on the other hand, went through a minimum at C33. This behavior can be rationalized in terms of the film morphology observed in the SEM images (Figure 6B–D). It can be seen that, at high Fe concentration, relatively large Fe clusters were formed on the substrate. It appears that the high concentration of ferritin precursor not only decreases the transparency but also reduced the concentration of nanotubes formed. Instead of the tight network observed at intermediate Fe concentrations, a relatively sparse structure with an apparent surface density of ~40 tubes/μm^2 is obtained at high concentrations. At the lowest concentration end, very small catalyst particles were formed after annealing. As can be compared in Figure 6B and C, no catalyst particles are visible on the sample made with C5 solution while they are clearly observed on the one made with C33 solution. As discussed earlier, smaller particles generate small diameter nanotubes, which are more easily hindered by interaction with other tubes and terminate growth more quickly. As a result, shorter tubes are produced, evidenced by a larger number of tube tips but lower tube density (i.e. ~7 tubes/μm^2) observed in the image. Therefore, on the film made with the C5 solution, a higher transparency but lower conductivity were obtained compared to that made with C33 solution. The C33 film, on the other hand, has a tube density as high as ~70 tubes/μm^2.

It is also worth noting that the C33-A60-Rz sample of this series showed higher conductivity and lower transmittance than the C33-A60-Rz sample of the annealing series. This difference can be ascribed to the additional 10 min of reaction that the latter underwent. This result indicates that reaction time is another important parameter that one can use to optimize film performance.

A popular method used by researchers to quantify performance of transparent conducting electrodes (TCE) is based on the following equation [37]:

$$T = \left(1 + \frac{1}{2R_s}\sqrt{\frac{\mu_0}{\varepsilon_0}}\frac{\sigma_{op}}{\sigma_{dc}}\right)^{-2}$$

Where T is the transparency measured at 550 nm, R_S the sheet resistance, σ_{dc} the electrical conductivity, σ_{op} the optical conductivity, $\mu_0 = 4\pi \times 10^{-7} NA^{-2}$ the free space permeability, and $\varepsilon_0 = 8.8542 \times 10^{-12} C^2 N^{-1} m^{-2}$ the free space permittivity. For a given sheet resistance, the lower is the value of the σ_{op}/σ_{dc} ratio, the higher is the transparency of the film. Therefore, films with low σ_{op}/σ_{dc} ratios are good candidates for TCEs. For example, to reach a sheet resistance of 15 kΩ/sq at a transparency of 98% the required ratio is 2.5. However, to increase the transparency to 99.5%, the ratio should decrease to 0.15.

The σ_{op}/σ_{dc} ratios obtained for the two series in this study are listed in Table 1. We compared transparency-sheet resistance data reported in several recent publications on transparent conductive SWCNT films (Table S1) with those in this study. While small ratios have been obtained in the intermediate transparency region, in the

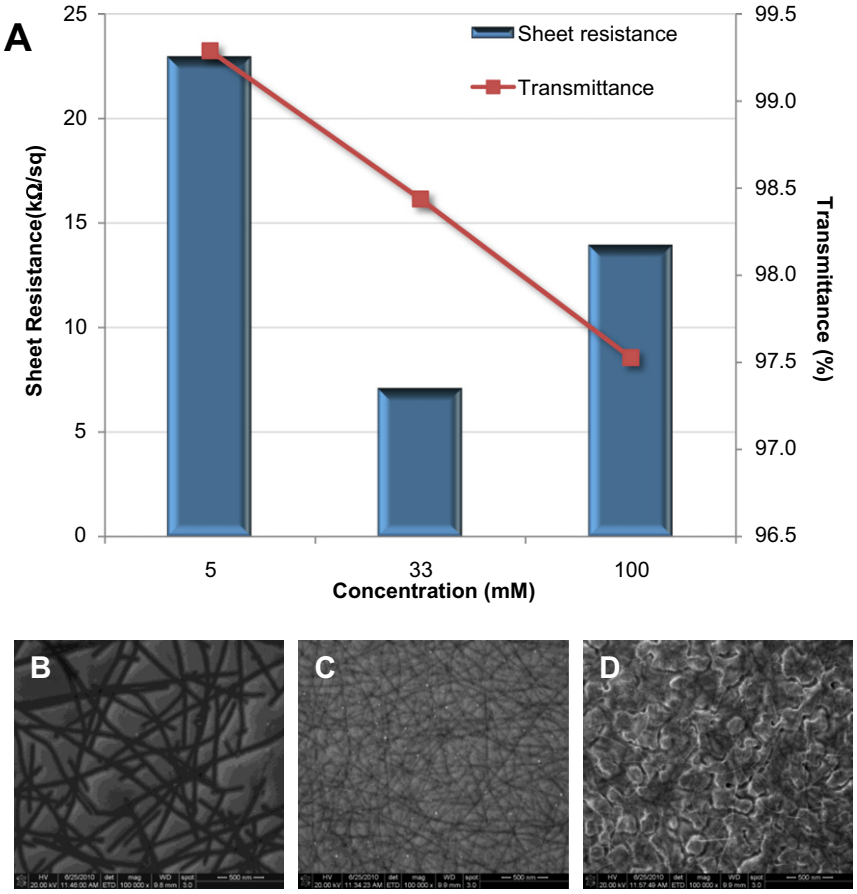

Figure 6. Sheet resistance and transmittance (at 550 nm) as a function of ferritin concentration and their corresponding SEM images. The samples were annealed for 60 min and reaction lasted for 30 min.

Table 1
σ_{op}/σ_{dc} values of the samples from this study.

Sample Name	σ_{op}/σ_{dc}
Annealing Series	
C33-A10-R20	0.36
C33-A20-R20	0.21
C33-A30-R20	0.25
C33-A45-R20	0.24
C33-A60-R20	0.23
Concentration Series	
C100-A60-R30	0.93
C33-A60-R30	0.30
C5-A60-R30	0.44

ultra-high transparency region, open circuit are often observed (i.e. σ_{op}/σ_{dc} infinitely large). By contrast, the films reported in this contribution for the annealing series have transparencies above 99% and σ_{op}/σ_{dc} ratios with an average of 0.26. Figure 7 shows the results of the annealing series along with some data extracted from recent literature. Using the average σ_{op}/σ_{dc} ratio of 0.26 one can extrapolate the high transparency data to the lower range for comparison with the less transparent films.

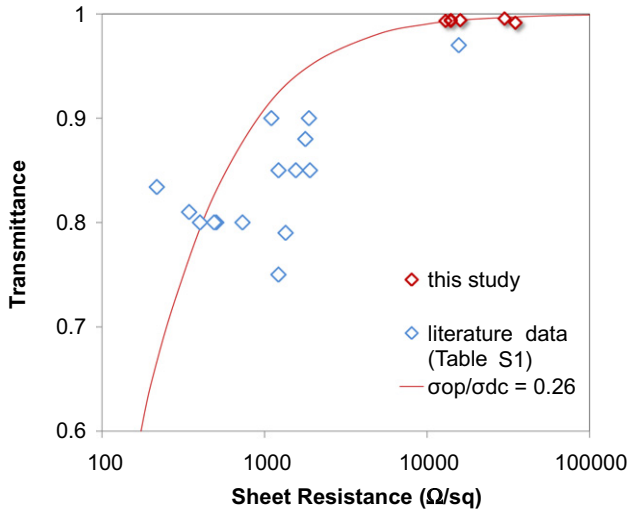

Figure 7. Transmittance vs. sheet resistance in this study and literature.

4. Conclusions

We have synthesized conductive SWCNT films with ultra-high transparency on transparent support. The high conductivity and transparency are attributed to the intrinsic advantages of the in situ procedure (as compared with methods based on deposition from solution) that resulted in long and unbundled nanotubes.

Acknowledgments

The project was financially supported by the Department of Energy-Basic Energy Sciences (Grants DEFG03-02ER15345 and DE-

FG02-06ER64239) and the Oklahoma State Regents for Higher Education. Spin-coating was carried out in Prof. David W. Schmidtke's lab. SEM characterization was conducted at the Oklahoma State University Microscopy Laboratory.

Appendix A. Supplementary data

Supplementary data associated with this article can be found, in the online version, at doi:10.1016/j.cplett.2011.06.057.

References

[1] J. Cui, A. Wang, N.L. Edleman, J. Ni, P. Lee, N.R. Armstrong, T.J. Marks, Adv. Mater. 13 (2001) 1476.
[2] L. Hu, D.S. Hecht, G. Gruner, Nano Lett. 4 (2004) 2513.
[3] Y. Zhou, L. Hu, G. Grüner, Appl. Phys. Lett. 88 (2006) 123109.
[4] Z. Wu et al., Science 305 (2004) 1273.
[5] A.A. Green, M.C. Hersam, Nano Lett. 8 (2008) 1417.
[6] H. Geng, K.K. Kim, K.P. So, Y.S. Lee, Y. Chang, Y.H. Lee, J. Am. Chem. Soc. 129 (2007) 7758.
[7] M.E. Spotnitz, D. Ryan, H.A. Stone, J. Mater. Chem. 14 (2004) 1299.
[8] T.V. Sreekumar, T. Liu, S. Kumar, L.M. Ericson, R.H. Hauge, R.E. Smalley, Chem. Mater. 15 (2003) 175.
[9] Y. Wang et al., Adv. Mater. 20 (2008) 4442.
[10] S.J. Kang et al., Nat. Nanotechnol. 2 (2007) 230.
[11] N. Ishigami, H. Ago, K. Imamoto, M. Tsuji, K. Iakoubovskii, N. Minami, J. Am. Chem. Soc. 130 (2008) 9918.
[12] D. Yuan, L. Ding, H. Chu, Y. Feng, T.P. McNicholas, J. Liu, Nano Lett. 8 (2008) 2576.
[13] S. Kim et al., Adv. Mater. 20 (2008) 1.
[14] J. Hone et al., Appl. Phys. Lett. 77 (2000) 666.
[15] J.E. Fischer, H. Dai, A. Thess, R. Lee, N.M. Hanjani, D.L. Dehaas, R.E. Smalley, Phys. Rev. B 55 (1997) 4921.
[16] P.B. Amama, M.R. Maschmann, T.S. Fisher, T.D. Sands, J. Phys. Chem. B 110 (2006) 10636.
[17] L. Durrer, T. Helbling, C. Zenger, A. Jungen, C. Stampfer, C. Hierold, Sens. Actuat. B 132 (2008) 485.
[18] I. Wako, T. Chokan, D. Takagi, S. Chiashi, Y. Homma, Chem. Phys. Lett. 449 (2007) 309.
[19] C. Kocabas, S. Hur, A. Gaur, M.A. Meitl, M. Shim, J.A. Rogers, Small 1 (2005) 1110.
[20] S. Han, X. Liu, C. Zhou, J. Am. Chem. Soc. 127 (2005) 5294.
[21] J.P. Edgeworth, N.R. Wilson, J.V. Macpherson, Small 3 (2007) 860.
[22] B. Kong, D. Jung, S. Oh, C. Han, H. Jung, J. Phys. Chem. C 111 (2007) 8377.
[23] W. Zhou, X. Bai, E. Wang, S. Xie, Adv. Mater. 21 (2009) 4565.
[24] G.T. Pham et al., Nanotechnology 19 (2008) 325705.
[25] D. Simien, J.A. Fagan, W. Luo, J.F. Douglas, K. Migler, J. Obrzut, ACS Nano 2 (2008) 1879.
[26] D. Hecht, L. Hu, G. Grüner, Appl. Phys. Lett. 89 (2006) 133112.
[27] P.E. Lyons, S. De, F. Blighe, V. Nicolosi, L.F.C. Pereira, M.S. Ferreira, J.N. Coleman, J. Appl. Phys. 104 (2008) 044302.
[28] P.N. Nirmalraj, P.E. Lyons, S. De, J.N. Coleman, J.J. Boland, Nano Lett. 9 (2009) 3890.
[29] A. Reina, M. Hofmann, D. Zhu, J. Kong, J. Phys. Chem. C 111 (2007) 7292.
[30] D. Shi, W.D. Tennyson, J. Keay, E. Sanchez, M.B. Johnson, D.E. Resasco, unpublished.
[31] A. Monzon, G. Lolli, S. Cosma, S.A. Mohamed, D.E. Resasco, J. Nanosci. Nanotechnol. 8 (2008) 6141.
[32] T. Thomson, S.L. Lee, M.F. Toney, C.D. Dewhurst, F.Y. Ogrin, C.J. Oates, S. Sun, Phys. Rev. B. 72 (2005) 064441.
[33] W.E. Alvarez, F. Pompeo, J.E. Herrera, L. Balzano, D.E. Resasco, Chem. Mater. 14 (2002) 1853.
[34] Y. Li, W. Kim, Y. Zhang, M. Rolandi, D. Wang, H. Dai, J. Phys. Chem. B 105 (2001) 11424.
[35] C. Cheung, A. Kurtz, H. Park, C.M. Lieber, J. Phys. Chem. B 106 (2002) 2429.
[36] W. Kim, A. Javey, R. Tu, J. Cao, Q. Wang, H. Dai, Appl. Phys. Lett. 87 (2005) 173101.
[37] M. Dressel, G. Gruner, Electrodynamics of Solids: Optical Properties of Electrons in Matter, Cambridge University Press, Cambridge, 2002.